Thrust Performance of Magneto Plasma Sail with a Magnetic Nozzle

IEPC-2015-329／ISTS-2015-b-329

Presented at Joint Conference of 30th International Symposium on Space Technology and Science
34th International Electric Propulsion Conference and 6th Nano-satellite Symposium,
Hyogo-Kobe, Japan
July 4 – 10, 2015

Yoshihiro Kajimura[1] and Tatsumasa Hagiwara[2]
Akashi National College of Technology, Akashi, Hyogo, 674-8501 Japan

Yuya Oshio[3] and Ikkoh Funaki[4]
Institute of Space and Astronautical Science, JAXA, Sagamihara, 252-5210 Japan

and

Hiroshi Yamakawa[5]
Research Institute for Sustainable Humanosphere, Kyoto University, Kyoto, 611-0011 Japan

Abstract: Magneto Plasma Sail (MPS) is a propulsion system used in space, which generates its force by the interaction between solar wind and an inflated magnetic field via plasma injection. In the present study, the quantitative evaluation of the thrust gain of the MPS with a magnetic nozzle has been conducted by using the ground experiment and the numerical simulation by three-dimensional hybrid particle-in-cell (PIC) simulations in an ion inertia scale. The optimized injected thermal plasma β is 2 and the ratio of Larmor radius of injected ion to the representative length of the magnetic field is one at the injection point. In this situation, the maximum thrust gain of the MPS with the magnetic nozzle is optimized numerically 24 compared with the thrust obtained by the pure magnetic sail. The thrust measurement of the MPS with this magnetic nozzle by using a pendulum type thrust stand experimentally has been conducted for verifying the concept of the thrust increase in the MPS with the magnetic nozzle.

Nomenclature

B = magnetic flux density, T
c = light velocity, m/s
F = thrust in plasma flow direction, N
J = current density vector (= $(1/\mu_0) \times$ rot B), J/m^2
L = representative size of magnetosphere, m
L_B = representative length of the magnetic field, m
M = magnetic moment, Tm^3
m = mass of Proton, kg
n = number density, m^{-3}

[1] Associate Professor, Department of Electrical and Computer Engineering, kajimura@akashi.ac.jp
[2] Advanced Course Student, Department of Mechanical and Electronic System Engineering, me1511@s.akashi.ac.jp
[3] Project Researcher, Institute of Space and Astronautical Science, y-oshio@ac.jaxa.jp.
[4] Associate Professor, Institute of Space and Astronautical Science, funaki@isas.jaxa.jp
[5] Professor, Research Institute for Sustainable Humanosphere, yamakawa@rish.kyoto-u.ac.jp

r_L = Larmor radius of plasma (ion) at the magnetopause, m
r_{Linj} = Larmor radius of injected plasma (ion) at the injection point, m
T = temperature, eV
v = velocity, m/s
v_{re} = relative velocity of plasma flow and neutral flow, m/s
σ = momentum-transfer cross section, m^2
μ_0 = permeability in vacuum
ω_{pi} = ion plasma frequency, 1/s
ω_{ci} = ion cyclotron frequency, 1/s

Subscripts

e = electron
i = ion
n = neutral
sw = solar wind plasma

I. Introduction

A new space propulsion system which is able to realize a better thrust performance namely higher specific impulse and larger thrust to power ratio than those of ion or hall thrusters must be developed in order to shorten the mission time to deep space. In order to achieve these requirements, one idea is to use the natural energy in space or to use an effective external energy source. Typical example of such space propulsion system using an external natural energy is Magneto Plasma Sail (MPS) [1]. MPS generates a propulsive force by the interaction between the solar wind and an artificially generated magnetic field inflated by the plasma injection from the spacecraft. When the plasma is injected, an initial magnetic field inflates to a position where the dynamic pressure of the solar wind and the magnetic pressure, including the dynamic pressure of injecting plasma, are balanced. Then, the MPS spacecraft generates a propulsive force by the interaction between the extensive magnetosphere and the solar wind. The schematic illustration of the MPS is shown in Fig.1. On the magnetosphere boundary surface, an induction current is induced in order to achieve balance between the pressure of the magnetic field and the dynamic pressure of solar wind. According to the Biot-Savart law, this current generates a magnetic field around the coil. A Lorenz force is produced by the coil current and the generated magnetic field, which acts on the coil as a propulsive force. The thrust performance of the MPS under the optimized parameters associated with the injected plasma has ever been evaluated by using numerical simulation[2]. In the present study, the thrust evaluation of the MPS in case that the magnetic moment vector is parallel to the solar wind flow direction is conducted. This configuration is expected that the magnetic field generated by the hoop coil operates as a magnetic nozzle and also operates as the sail for obtaining the thrust from the solar wind. Conceptual illustration of the thrust generation mechanism in the magnetic nozzle is shown in Fig. 2. The magnetic nozzle would achieve a high exhaust velocity, namely high propellant utilization efficiency, since plasma would not contact wall structures directly when the plasma was exhausted from the nozzle. As other propulsion systems using the magnetic nozzle, the Variable Specific Impulse Magnetoplasma Rocket (VASIMR) has been proposed and tested[3]. The rocket consists of a helicon plasma source and a combined system of ion cyclotron resonance heating (ICRH) and a magnetic nozzle. A diverging magnetic nozzle plays an important role in converting plasma thermal energy heated by ICRH to its flow energy. In Tohoku University, the combined experiments of ion cyclotron resonance heating and acceleration in the magnetic nozzle using fast-flowing plasma in the HITOP device[4] have also been performed. Under these research circumstances, a magnetic nozzle is a promising accelerator device for new advanced propulsion systems.

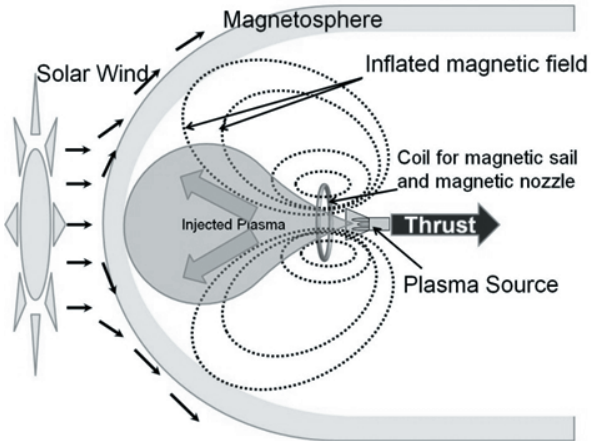

Figure 1. Schematic illustration of the MPS with the magnetic nozzle.

In the present research, the following two purposes of our study are listed. One is to optimize the injected plasma parameters for the thrust gain of the newly proposed propulsion system of the MPS with magnetic nozzle. Second one is to verify the concept of the thrust increase in the MPS with the magnetic nozzle numerically and experimentally by using a 3D hybrid Particle-in-Cell Simulation and a pendulum type thrust stand in the vacuum chamber, respectively.

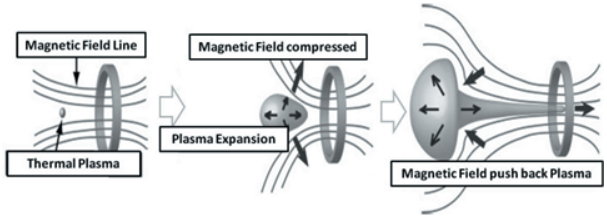

Figure 2. Conceptual illustration of thrust generation mechanism of the magnetic nozzle.

II. Numerical Simulation

A. Simulation Model

Figure 3 illustrates the simulation model. The coil of the MPS spacecraft is assumed to coincide with the origin of the simulation box. The radius of the coil and the coil current are set at the same values as those used in the supposed laboratory experiment, which are listed in Table 1. The initial distribution of the magnetic field with the magnetic nozzle shown in Fig. 3 is maintained in the simulation box. The representative length of the magnetosphere of L without thermal plasma injection is determined by the pressure balance between the dynamic pressure of the solar wind plasma and the magnetic pressure. The L as shown in Fig. 3 is results from Eq. (1).

$$L = \sqrt[6]{\frac{\mu_0 M^2}{8\pi^2 n_{sw} m_i v_{sw}^{\ 2}}} \tag{1}$$

The parameters associated with the plasma flow are set to the values listed in Table 1. Initially, the proton ions, indicated with an arrow (solar wind plasma) in Fig. 3, are injected from the side of the $-Z$ boundary. The ions are injected from that region of the boundary which has a finite thickness of $v_{sw} \times dt$ and are then located randomly in that finite region. The velocity distribution of ion follows a Maxwellian distribution. After the solar wind and thermal plasma injection is initiated, the simulation is continued till the magnetosphere formed attains a steady-state.

The parameters of the injected thermal plasma for the thrust optimization are listed in Table 2. The variable angle θ shown in Fig. 3 corresponds to optimize the distance between the injected thermal plasma location and the center of the coil. Also the variable range of the injected thermal plasma parameters for the thrust optimization, the density, ion temperature and mass flow rate are listed in Table 2. In Table 2, r_{Linj}/L_B and β are the ratio of Larmor radius of injected ion to the representative length of the magnetic field ($|B/(\partial B/\partial x)|$) and the ratio of plasma thermal pressure to magnetic pressure at the injection point, respectively.

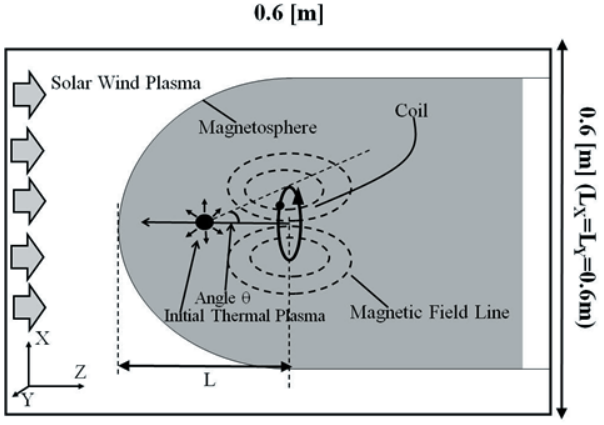

Figure 3. Simulation Model.

B. Simulation Code

The 3D hybrid PIC model used in the present study is based on the model proposed by Horowitz[5]. The hybrid particle-in-cell (PIC) model treats ions as individual particles and electrons as a fluid. This approach is valid when the system behavior is dominated by ion physics. The leap-frog method[5] is adopted to solve the equation of motion of the ions. We assume a quasi-neutrality condition and set the ion charge density equal to the electron charge density. We introduce the Darwin approximation[5] in the equation of Ampere's law. To carry out stable calculations in relatively low density plasma and strong magnetic field, we adopt the CAM-CL (Current Advance Method and

Cyclic Leapfrog) method[6]. In vacuum region, the electric field is calculated from the Laplace equation ($\nabla^2 \boldsymbol{E} = 0$) using the successive over relaxation (SOR) numerical method[7]. A density threshold is assigned to distinguish the plasma region from the vacuum region; if the density of the plasma in a region is less than 20% of that of the solar wind plasma flow, then that region is considered as a vacuum region. During the simulation, the electron temperature is kept constant. Cartesian coordinates (X, Y, Z) are adopted and the zero-gradient condition in the electric and magnetic field is adopted at the boundary.

Table 1. Simulation Parameters.

Parameters	Simulation Parameters (Base)
Solar Wind Parameters	
Injection Plasma	Hydrogen
Velocity : u_{sw}	28 [km/s]
Density : n_{sw}	1.0e+18[m^{-3}]
Electron Temperature : T_e	0.84[eV]
Ion Temperature : T_i	0.84[eV]
Coil Parameters	
Coil Radius	0.075 [m]
Coil Current	3.6 [kA turn]
B-field at the Center of Coil	0.03 [T]
Theoretical:L (Magnetic Cavity Size)	0.2 [m]
Ratio of Ion Lamor Radius to L	1.67
Ionization Ratio	0.3
Simulation Parameters	
dx	0.05 c/ω_{pi}
dt	0.01 ($1/\omega_{ci}$)
Number of Particles per Cel	50 /cell
Mesh Number	60*60*60

C. Collision Model

The degree of ionization α is defined as the ratio of the n_{sw} to the density of ion and neutral gas ($n_{sw} + n_n$). The degree of ionization α of 0.3 is used in the present simulation, which value was decided based on the past evaluation[8]. Most of the hydrogen molecules (H_2) dissociate into atoms (H) at a relatively high temperature of 1 eV. (at 0.5 eV, 95% dissociation). The ratio of the mean free path of H-H^+ momentum transfer collision and the $L\sim$ 0.1 m is on the order of one. Therefore, the effect of the collision between the H and H^+ must be taken into consideration in the numerical simulation. A Monte Carlo collision model is adopted as the elastic and momentum-transfer collision model in the PIC method[9]. When the collision occurs, the velocity of ion is calculated by the same method in Ref. 9. The hydrogen atoms with Maxwellian distribution are assumed to be distributed throughout the simulation region.

$$P_{collision} = 1 - \exp\left(-n_n \sigma \cdot v_{re} \cdot \Delta t\right) \tag{2}$$

The n_n is calculated from α and n_{sw}. The momentum-transfer cross section of an elastic collision depends on the relative velocity between the hydrogen ion and atom. This cross section is calculated from the experimental data reported in Ref. 10, and this value is set to be constant throughout the simulation. A probability of the occurrence of the collision is calculated from Eq. (2), where σ is the momentum-transfer cross section, and v_{re} is the relative velocity between the hydrogen ion and atom. The collision parameters are summarized in Table 3. 50% of all collisions are treated as the charge exchange collisions described in Ref. 11.

Table 2. Parameters for the thrust optimization.

Parameters for optimization	
Thermal Plasma Parameters	
Injection Plasma	Hydrogen
Location θ	0～90 [deg]
Density : n_{inj}	5.0e+18～5.0e+21[m^{-3}]
Velocity : u_{inj}	38 [km/s]
Ion Temperature : T_i	0.84～840 [eV]
Mass Flow Rate	0.1～100 [mg/s]
r_{Linj}/L_B	3～100
β	1e-3～1e+3

Table 3. Collision model parameters.

Collision Model Parameters	
Ionization Ratio α	0.3
Momentum Transfer Cross Section (H^-+H)[10]	4e-19 [m^2]
Neutral Density	9.92e+19 [m^{-3}]
Neutral Velocity	16 [km/s]

III. Numerical Simulation Results and Discussion

A. Optimized Parameters of Thermal Injected Plasma

The location of the injected thermal plasma has been optimized using the same hybrid PIC model1[2]. The maximum momentum conversion ratio using the magnetic nozzle under the same configuration of the present study reached 70 % in case for $\theta = 45$ degrees[12]. In the present simulation, the location of the initial thermal plasma is fixed value for $\theta = 45$ degrees. Figure 4 shows how the thrust gain (F_{inj}/F_0, F_{inj} : thrust value with injected plasma, F_0 : thrust value without injected plasma) obtained from the MPS with the magnetic nozzle depends on r_{Linj}/L_B and thermal β at the injection point. In the present numerical simulation, the Maxwell stress generated on the coil is calculated from the simulation results. The calculated Maxwell stress includes both the thrust for the magnetic nozzle and the thrust for the MPS. When r_{Linj}/L_B is around unity, the thrust gain becomes large gradually increasing the thermal plasma β since expanding ions with small gyro radius are reflected by the magnetic nozzle effectively. On the other hands when r_{Linj}/L_B is greater than unity, the interactions between ions and magnetic nozzle becomes weak and reduces the thrust obtained, since the finite ion Larmor radius effect appears in this interaction. It found that the maximum thrust gain obtained from the MPS with magnetic nozzle was 24 in case for $r_{Linj}/L_B = 1$ and thermal plasma $\beta = 2$ as shown in Fig. 4. However the present optimized injected plasma parameter for $\beta = 2$, $r_{Linj}/L_B = 1$ is unrealistic for realizing in the ground experiment since the number density for this parameter is 10^{24} [/m^3]. So the available parameter $\beta = 0.46$, $r_{Linj}/L_B = 3$ for the plasma injection in the ground experiment using the vacuum chamber is selected from the parameters in the numerical investigation which is indicated by a black circle as shown in Fig. 4. In the next section, the simulation results for the case of $\beta = 0.46$, $r_{Linj}/L_B = 3$ is shown.

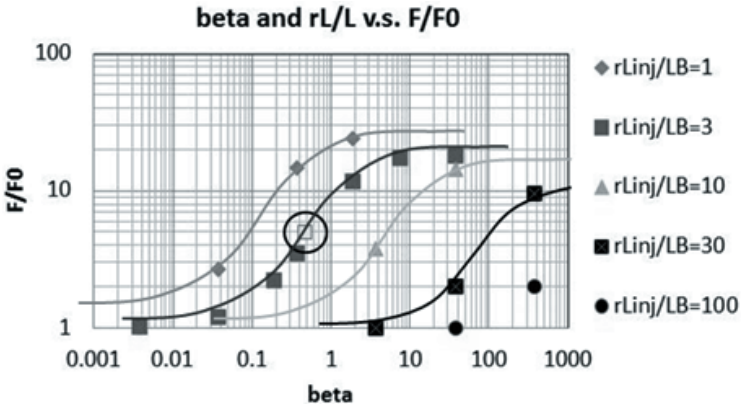

Figure 4. Thrust gain F_{inj}/F_0 of MPS versus initial thermal plasma β and r_{Linj}/L_B for $\theta = 45$ deg.

B. Number Density Distribution of Plasma (Ions)

Figure 5a and 5b show the simulation results of the contour plot of the averaged ion density distribution and magnetic field line on XZ plane w/o injected thermal plasma (5a) and with injected thermal plasma (5b). Figure 5b corresponds to the result obtaining the thrust gain 5 for $r_{Linj}/L_B = 3$ and thermal plasma $\beta = 0.46$ as shown in Fig. 4. In Fig. 5a, a relatively low-density region is seen in the wake regions behind the coil and the relatively high-density

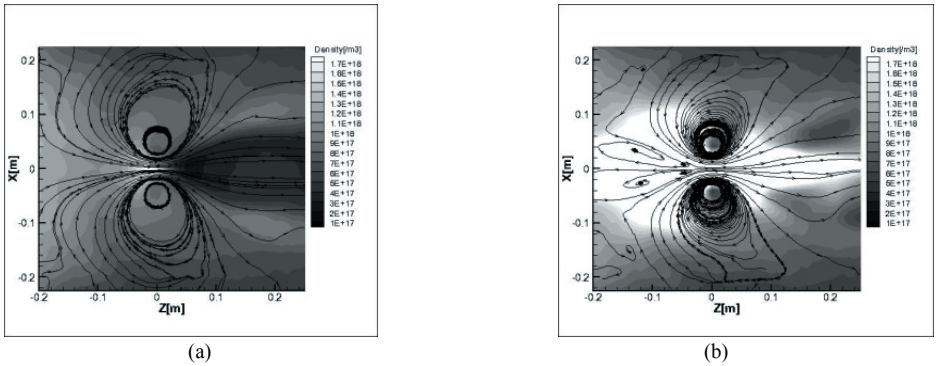

(a) (b)

Figure 5. Simulation results of the contour plot of the averaged ion density distribution and magnetic field line on *XZ* plane w/o injected thermal plasma (a) and with injected thermal plasma (b).

region in the magnetic cusp can be seen in Fig. 5a. Ion particles of solar wind plasma are reflected with gyro motion at the magnetopause due to $\boldsymbol{J} \times \boldsymbol{B}$, and then the magnetosphere is formed in the steady state. However it is not clearly seen the magnetosphere in Figs. 5 since the interaction between the solar wind plasma flow and the magnetosphere is weak under the supposed experimental condition for r_L/L=1.67. The injected thermal plasma with injected velocity is expanded almost isotropically, and then the ions in the direction of the coil are reflected back by the magnetic nozzle, and its shape changes to follow the dipole magnetic field line. In Fig. 5b, one can see the high density region where the plasma is accelerated away from the coil due to the magnetic nozzle.

To quantitatively compare the simulation results with injected thermal plasma and w/o injected thermal plasma, the profile of the magnetic flux density along the X and Z-direction on the coil center, the B_z is plotted, as shown in Figs. 6a and 6b. The vertical axis in Figs. 6a and 6b represent the magnetic flux density of the Z-component (B_z). The value of B_z with and w/o injected plasma starts to increase near the position of magnetosphere boundary since the unperturbed magnetosphere was compressed by the solar wind plasma flow. If the thermal plasma is injected, the injected plasma is reflected by the magnetic nozzle and the plasma is accelerated away from the coil. Simultaneously, the induced current is generated by the ejected plasma away from the magnetic nozzle. This current is induced by the plasma with grad B drift motion having the same direction as the original coil current. Figure 7 shows the contour plot of the ion current density distribution as obtained by the simulation. On interaction with the magnetic field, the injected thermal ion moves to the ±Y-direction (perpendicular to the plane in Fig. 7) due to a gyro motion, resulting in the formation of the magnetic sail inflation as shown in Figs. 6a and 6b. The location of the cross point (shown as the dotted line in Fig. 6a) between the initial profile and the profile in steady state result corresponds to the magnetosphere boundary. It can be seen that the location of the cross point in Fig. 6a namely the magnetosphere expands clearly due to the current induced by the momentum transfer of the thermal plasma by the magnetic nozzle. Also in Fig. 6b, the magnetic flux density on Z-direction increases due to the grad B drift current namely ring current induced by the magnetic nozzle. The thrust increment of the MPS with the magnetic nozzle was observed in the simulation results, which indicates that the magnetosphere expanded due to magnetic inflation. This combination merit corresponds to the concept of the MPS with magnetic nozzle.

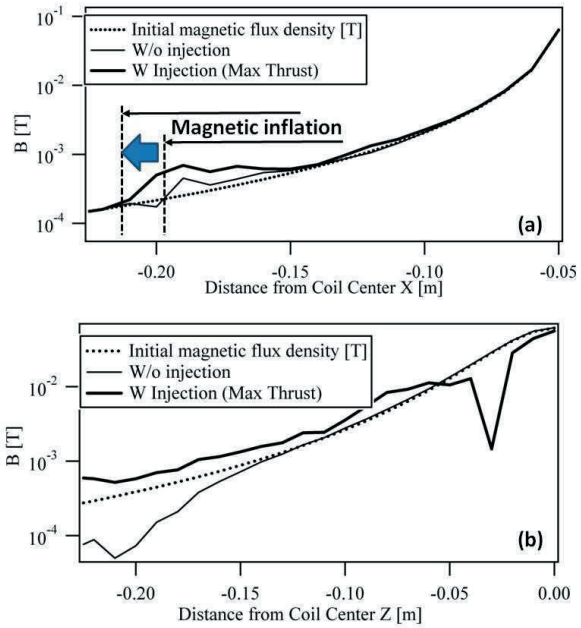

Figure 6. Simulated magnetic flux density profile along X and Z-direction obtained w/o injected plasma and with injected plasma in case for r_{Linj}/L_B = 3 and thermal plasma β = 0.46.

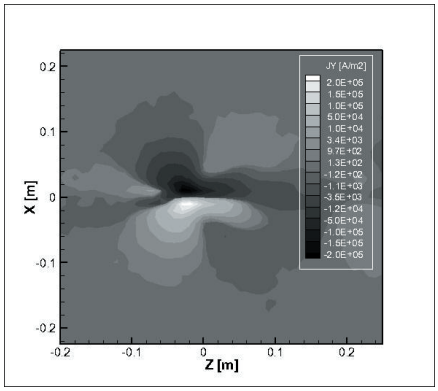

Figure 7. Contour plot of ion current density distribution J_y on XZ-plane with injected thermal plasma in case for r_{Linj}/L_B = 3 and thermal plasma β = 0.46.

IV. Ground Experiment for the thrust measurement of the MPS with magnetic nozzle

A. Experimental Setup

The experimental set up for the direct thrust measurement of the MPS with a magnetic nozzle thruster using a vacuum chamber is shown in Fig. 8. The experiment devices consist of Solar Wind Simulator (MPD_SWS), the magneto plasma sail thrust stand, operating and measuring system. The thrust stand consists of MPD Arcjet for injecting plasma, the solenoid coil for generating magnetic nozzle and magnetic sail and aluminum bar suspended by four stainless wires. Solar Wind Simulator generates hydrogen (H^+) plasma with 38 km/s as the solar wind plasma flow. And plasma injection source injecting near the center of the coil utilizes for the increase of the thrust due to magnetic nozzle and for inflating of the magnetic sail. Magneto Plasma Dynamic Arcjet (MPD) is also used as plasma injection source (Plasma injector). When the solenoid coil, the plasma injector and the MPD_SWS operate at the same time, it occurs the interaction between the magnetic field and the injected plasma which ignites finite time duration of approximately 1 ms. This experiment has been conducted under three situations. First one is the magnetic sail mode which operates the MPD_SWS and the solenoid coil. Second one is the magnetic nozzle mode which operates the solenoid coil and the plasma injector. Last one is the magneto plasma sail with magnetic nozzle mode which operates the MPD_SWS, the solenoid coil and the plasma injector. The magneto plasma sail with magnetic nozzle mode combined the magnetic sail mode and the magnetic nozzle mode. The displacement of the thrust stand is detected by the laser and the resulting displacement plot is displayed on the scope coder. Parameters used in the present ground experiment are shown in Table 3.

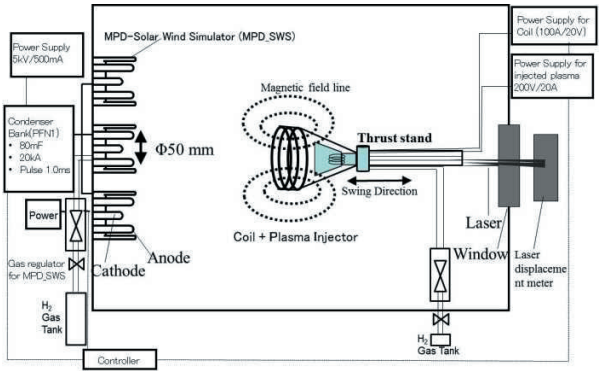

Figure 8. Experimental set up for the direct thrust measurement of the MPS with a magnetic nozzle thruster.

Table 3. Parameters used in the ground experiment.

Solar Wind Simulator Parameters	
Density	1.0e+18[m^{-3}]
Velocity	28[km/s]
Temperature	0.84[eV]
Plasma Injection Source Parameters	
Density	5.0e+20[m^{-3}]
Mass Flow Rate	20[mg/s]
Temperature	0.84[eV]
Solenoid Coil Parameters	
Current	3.6[kA turn]
Turn	20
Radius	0.075[m]
B-field	0.03[T]

B. Experimental Result of the photographs taken by a shutter camera

In the present experiment, the measurement of not only the thrust for the magneto plasma sail with magnetic nozzle but also the photograph of the interaction between the magnetic field and the plasma flow are conducted. The photographs in case for each operation in the experiment are shown in from Fig. 9 to Fig. 11.

Figure 9 shows the photograph of the plasma flow taken using a shutter camera around the magnetic sail. When the photographs are taken, a shutter of camera keeps opening in a second. The simulated solar wind flows from the left boundary. As shown in Fig. 9, the solar wind plasma changes the ionization plasma into the de-ionization one by colliding directly to the solenoid coil. In this process, it emitted the light depending on the plasma density. The relatively bright region near the center of coil can be seen in Fig. 9. This is because the injected plasma from the MPD_SWS was collected in the center of the solenoid coil due to the shape of magnetic cusp generated by the solenoid coil. Figure 10 shows the photograph in case for the magnetic nozzle mode. The plasma is injecting from MPD injector with high injection velocity of 38 km/s plus thermal velocity of 0.84 eV. As shown in Fig. 10, the luminescence intensity is so strong compared with magnetic sail mode which already shown in Fig. 9. The plasma injected from MPD injector is concentrated at the center of the solenoid coil by the magnetic nozzle generated by the solenoid coil. This is the action due to the magnetic nozzle. Figure 11 shows the photograph in case for the magneto

plasma sail with magnetic nozzle mode. The simulated solar wind flows from the left boundary. When the solar wind simulator run at the same condition of magnetic nozzle mode, the injected plasma from MPD has a little expansion compared with the magnetic nozzle mode which already shown in Fig. 10. This is because the magnetic nozzle and the injected plasma from injector are both compressed simultaneously by the plasma injected from MPD_SWS as shown in Fig. 11. In this process, it is expected that the shape of magnetic nozzle is inflated due to the deformation of magnetic sail by the grad B drift current induced by the plasma injected from MPD injector as mentioned using numerical simulation results in the Section 3.

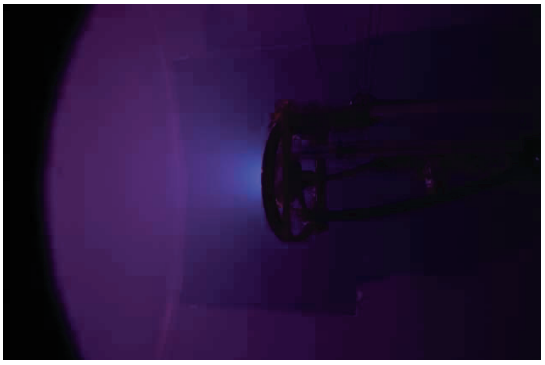

Figure 9. Time exposure photograph of interaction between the solar wind plasma and the magnetic field (Experimental result in case for the magnetic sail mode: solar wind simulator + solenoid coil).

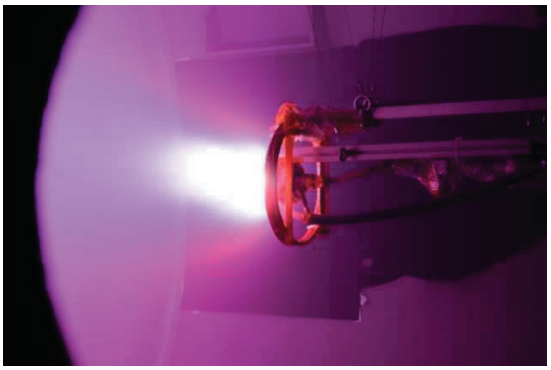

Figure 10. Time exposure photograph of interaction between the injected plasma and the magnetic field (Experimental result in case for the magnetic nozzle mode: solenoid coil + plasma injector).

Figure 11. Time exposure photograph of interaction between the injected plasma and the magnetic field (Experimental result in case for the magneto plasma sail with magnetic nozzle mode:magnetic sail + magnetic nozzle).

C. Experimental Result of the thrust in each case

The measured thrust is evaluated from the displacement of the thrust stand in each mode. The results of measured thrust are shown in Fig. 12.

$$\text{(Thrust in case for the magnetic sail)} = (F_{\_Coil+SWS})-(F_{\_Coil})-(F_{\_SWS}) \tag{3}$$

$$\text{(Thrust in case for the magnetic nozzle)} = (F_{\_Coil+MPD})-(F_{\_Coil})-(F_{\_MPD}) - \text{(The interaction between coil and MPD)} \tag{4}$$

(Thrust in case for the magneto plasma sail with magnetic nozzle)
$= (F_{\_Coil+SWS+MPD}) - (F_{\_Coil}) - (F_{\_SWS}) - (F_{\_MPD})$-(The interaction between coil and MPD) (5)

The evaluation method for the measurement of the thrust in each mode is shown below. In case for the magnetic sail mode, the displacement of the thrust stand attached with the coil under the magnetic sail mode is measured by the laser displacement meter. Then the above measured value minus the displacement of the thrust stand only operating the MPD_SWS and minus the displacement only operating the coil as shown in Eq.(3). The obtained thrust in case for the magnetic sail mode shows at the bottom of Fig.11 as ①. As shown in Fig. 11, the obtained thrust in case for the magnetic sail is approximately 0.5 N. By using Eq. (4), the obtained thrust is approximately 2.7 N in case for the magnetic nozzle mode as shown for ② in Fig.11. The obtained thrust for the sum of the thrust in case for the magnetic sail mode simply plus the case for the thrust of the magnetic nozzle mode is approximately 3.1 N. The electromagnetic interaction between the coil and injector (MPD) is evaluated by the displacement due to the attraction and repulsion by changing the current direction of the coil. In case for the magneto plasma sail with magnetic nozzle mode, the coil, the SWS_MPD and injector operate at the same time. Then the displacement of the thrust stand attached with the coil is measured by the laser displacement meter. By using Eq. (5), the obtained thrust in case for the magneto plasma sail with magnetic nozzle mode shows at the top of Fig.11 as ③. The obtained thrust in case for the magneto plasma sail with magnetic nozzle mode is approximately 5.6 N. If the obtained thrust in case for the magneto plasma sail with magnetic nozzle mode is larger than the obtained thrust in case for the simple summation of the thrust of the magnetic sail and the thrust of the magnetic nozzle, the inflation of the magnetic sail is occurred in the configuration of the magnetic nozzle. It means that the obtained thrust from solar wind increase due to the expansion of the magnetic sail. This increase of the thrust is indicated the black bar as shown in Fig 11. This combination merit is the concept of the MPS with magnetic nozzle. These all measurements of the thrust are average value of three times measurements. The thrust for the magneto plasma sail with magnetic nozzle mode is approximately 12 times as large as the thrust for the magnetic sail mode. Furthermore, the thrust of magneto plasma sail with magnetic nozzle mode is approximately 2 times as large as the sum of the thrust of the magnetic sail mode plus the thrust of the magnetic nozzle mode.

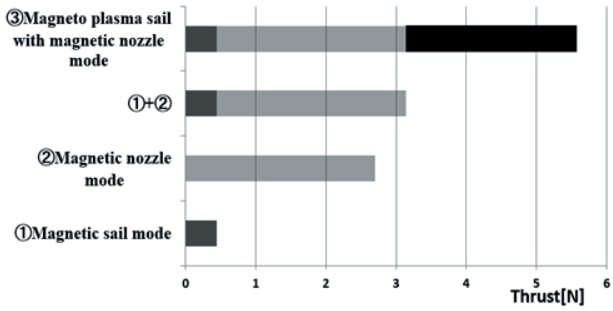

Figure 12. The experimental thrust measured in each mode.

V. Summary

The 3D hybrid particle-in-cell simulation was carried out by adopting a Monte Carlo collision model in order to optimize the thrust gain of the MPS with magnetic nozzle thruster for the ground experiment. The optimized injected thermal plasma β is 2 and the ratio of Larmor radius of injected ion to the representative length of the magnetic field is 1 at the injection point. In this situation, the maximum thrust gain of the MPS with the magnetic nozzle is 24 compared with the thrust obtained by the pure magnetic sail. The magnetic inflation was achieved by the loop-like current induced by the thermal plasma transferred the momentum by the magnetic nozzle. This current is induced by the plasma with grad B drift motion having the same direction as the original coil current. Also the thrust obtained by the magnetic nozzle was successfully observed. In order to confirm the principle of magneto plasma sail with magnetic nozzle, the laboratory experiment by using vacuum chamber have been conducted. The main purpose of the present experiment is to measure the thrust of the magneto plasma sail with magnetic nozzle by using a thrust stand hanging from the vacuum chamber ceiling. As experimental results, the thrust of magneto plasma sail is 2 times as large as the sum of the thrust of magnetic sail plus the thrust of magnetic nozzle. In the experiment, MPD is used as the plasma injection source for the magnetic nozzle thruster. This plasma injection source needs high electric power of MW class to generate the plasma. So, it's difficult to prepare high electric power because the energy is limited in the space. The next experiment will be planning to use the plasma source which is used the helicon waves and conduct the same experiment as the plasma source which utilizes the helicon waves

operates with lower electric power to generate the plasma. So, the helicon waves plasma source is expected the improving of thrust power ratio as the thrust system.

Acknowledgments

We gratefully acknowledge the support and advice of the MPS research group members in Japan. The present experiment was supported by the advanced plasma chamber in ISAS/JAXA (Japan Aerospace Exploration Agency). This research was also supported by the Ministry of Education, Science, Sports and Culture, Grant-in-Aid for Scientific Research (B), 2013-2014（No.24760669, Yoshihiro Kajimura. The computation in the present study was performed as a collaborative research project using the KDK system of the Research Institute for Sustainable Humanosphere (RISH) at Kyoto University.

References

[1]Winglee, R. M. et al., "Mini-Magnetospheric Plasma Propulsion: Tapping the Energy of the Solar Wind for Spacecraft Propulsion," *Journal of Geophysical Research*, Vol. 105, No. A9, (2000), pp. 21,067–21,077.

[2]Yoshihiro Kajimura et al., "Thrust Evaluation of Magneto Plasma Sail by Using Three-Dimensional Hybrid PIC Code," *Proc. of 46th AIAA/ASME/SAE/ASEE Joint Propulsion Conference*, AIAA 2010-6686, (2010).

[3]Chang Diaz, F. R., The VASIMR Rocket, Scientific American; 283 (5), (2000), P90.

[4]Ando, A., Inutake, M., Hattori, K., Shibata, M., and Kasashima, Y., ICRF Heating and Plasma Acceleration with an Open Magnetic Field for the Advanced Space Thruster, Transaction of Fusion Science and Technology, Vol. 51, No. 2T, 2007, pp. 72-74.

[5]Horowitz, J. E., Shumaker, D. E., and Anderson, D. V.: QN3D: A Three-Dimensional Quasi-Neutral Hybrid Particle-in-Cell Code with Applications to the Tilt Mode Instability in Field Reversed Configurations, *Journal of Computational Physics*, **84**, (1989), pp. 279–310.

[6]Matthews, A. P.: Current Advance Method and Cyclic Leapfrog for 2D Multispecies Hybrid Plasma Simulations, *Journal of Computational Physics*, **112**, (1994), pp. 102–116.

[7]Harned, D., S.: Quasineutral Hybrid Simulation of Macroscopic Plasma Phenomena, *Journal of Computational Physics*, **47**, 3, (1982), pp.452-462.

[8]Kajimura, Y., Usui, H., Funaki, I., Ueno, K., Numani, M., Shinohara, I., Nakamura, M., and Yamakawa, H.: 3D Hybrid Simulation of Pure Magnetic Sail including Ion-Neutral Collision Effect in Laboratory, *Journal of Propulsion and Power*, **26**, 1, (2010), pp. 159–165.

[9]Vahedi, V., and Surendra, M.: Monte-Carlo Collision Model for Particle-in-cell Method: Application to Argon and Oxygen discharge, *Computational Physics Communications*, **87**, (1995), pp. 179–198.

[10]Kristic, P. S., and Schultz, D. R.: Consistent Definitions for, and Relationships among Cross Sections for Elastic Scattering of Hydrogen Ions, Atoms, and Molecules, *Physical Review A*, **60**, 3, (1999), pp. 2118-2130.

[11]Golant, V. E., Zhilinsky, A. P., and Sakharovt, I. E.: *Fundamentals of Plasma Physics*, Chapter 2.6, (1977), pp. 46-49.

[12]Konstantin V. Vchivkov, Hideki Nakashima, Fumihiro Ichikawa, Yuri P. Zakharov, Optimization of thrust efficiency in laser fusion rocket by using three-dimensional hybrid particle-in-cell code, *Vacuum*, **73**, Issues 3–4, (2004), pp. 427–432.